jet INTL JOURNAL OF ELECTRONICS AND TELECOMMUNICATIONS, 2019, VOL. 65, NO. 2, PP. 277–286
Manuscript received December 20, 2019; revised April, 2019. DOI: 10.24425/ijet.2019.126311

Comparing Gausian and exact models of malicious interference in VLC systems

Grzegorz Blinowski, Adam Mościcki

***Abstract*—Visible Light Communication (VLC) is a technique for high-speed, low-cost wireless data transmission based on LED luminaries. Wireless LAN environments are a major application of VLC. In these environments, VLC is used in place of traditional systems such as Wi-Fi. Because of the physical characteristics of visible light, VLC is considered to be superior to traditional radio-based communication in terms of security. However, as in all wireless systems, the security of VLC with respect to eavesdropping, signal jamming and modification must be analyzed. This paper focuses on the aspect of jamming in VLC networks. In environments where multiple VLC transmitters are used, there is the possibility that one or more transmitters will be hostile (or "rogue"). This leads to communication disruption, and in some cases, the hijacking of the legitimate data stream. In this paper we present the theoretical system model that is used in simulations to evaluate various rogue transmission scenarios in a typical indoor environment. The typical approach used so far in jamming analysis assumes that all disruptive transmissions may be modeled as Gaussian noise, but this assumption may be too simplistic. We analyze and compare two models of VLC jamming: the simplified Gaussian and the exact model, where the full characteristics of the interfering signal are taken into account. Our aim is to determine which methodology is adequate for studying signal jamming in VLC systems.**

***Keywords*—Visible light communication networks, Network security, Physical layer security, Transmission jamming**

I. Introduction

VISIBLE light communication (VLC) was first proposed in the early 2000s [1]–[3]. It uses single LED or multiple-LED luminaries as the wireless transmitter and photodiodes or CMOS-sensor cameras as the receiver. The driving factor behind the development of VLC is the growing popularity of LED-based lightning. LED based luminaries are 60 – 80 % more energy efficient than incandescent and fluorescent light sources – hence more environmentally friendly. They are also more reliable (in terms of mean time before failure). In a VLC system, data is transmitted by rapidly switching the light source on and off or by modulating the intensity of the light source at a rate that is significantly higher than the perception limits of the human eye.

A. VLC – technology and applications

The throughput of VLC systems has significantly improved as new techniques for the transmitter and receiver design have been introduced: in the first experimental systems, data transmission in the range of 40 Mb/s was achieved [4], and 100-200 Mb/s has been demonstrated [5] with an improved single-emitter–single-receiver scenario and On-Off Keying. Data rates in the range of 1 Gbps were attained with Orthogonal Frequency Division Multiplexing (OFDM) [6] and arrays of separately driven light sources and multiple receivers (VLC MIMO) [7]. Recently, with the use of GaN violet micro-LEDs, a data transfer speed in the range of 10 Gb/s has been found to be achievable [8]. For more information on the development of VLC technology, we refer the reader to the survey papers by Pathak and Khan: [9], [10].

Significant applications of VLC technology have been proposed and implemented, some experimentally, while some have found commercial implementations, the most important being:

- peer-to-peer data exchange – such as between handheld devices,
- data broadcasting — for example in home audio and video streaming,
- multimedia conferencing,
- general data communication in personal and local wireless area networks (WPAN and WLAN),
- localization and navigation, both indoor (for example in large shopping centers, museums, etc. where GPS signal may be unavailable) and outdoor – where it can be integrated with traffic light system,
- targeted advertisement and communication,
- home automation, inventory management and asset tracking – which is related to the IoT environment,
- Vehicle Area Networks (VANETs) and intelligent transportation systems in vehicle-to-vehicle and vehicle-to-roadside communication.

More information on VLC applications may be found in: [6], [11]–[14]. In recent years, a lot of effort has been made to commercialize VLC technology. For example, PureLiFi Ltd. – founded by a pioneer of VLC research Harald Hass – developed a VLC Access Point "LiFi-X" – promoted as a replacement for a traditional Wi-Fi AP with an uplink and downlink data rate of 43 Mbps.

B. VLC security issues

Security requirements for VLC-based WLANs are not different from the general security requirements for other wireless systems. The aim is to protect data transmission against attacks such as eavesdropping, jamming, data modification, etc. The complete set of security requirements is often collectively

This work was supported by the Statutory Grant of the Polish Ministry of Science and Higher Education, given to the Institute of Computer Science, Warsaw University of Technology.

Grzegorz Blinowski and Adam Mościcki are with Institute of Computer Science, Faculty of Electronics and Information Technology, Warsaw University of Technology, Nowowiejska 15/19, 00-665 Warsaw, Poland (e-mail: g.blinowski@ii.pw.edu.pl).

presented as the **CIAA** suite, i.e.: Confidentiality, Integrity, Authenticity and Availability.

It is important to enumerate the key factors differentiating radio-based and light-based WLANs:

- VLC uses a broadcast channel, so in principle it is difficult to shield transmitted data from bystanders.
- In VLC WLANs, the Line-of-Sight (LoS) signal component is dominant over the Non-Line-of-Sight (NLoS) – this is in contrast to RF-based WLANs, therefore, signal reflection leading to multipath effects is far less significant in VLC.
- With current technology, it is not possible to use phase modulation in VLC systems. In effect, channel entropy in VLC systems is lower than in RF-based systems.
- Because of physical LEDs characteristics the modulating electrical current must fall within strict amplitude constraints (mainly to avoid nonlinear effects). Hence, intensity modulation (IM) and Direct Detection (DD) are used in VLC. The transmission channel is typically modeled with amplitude constraints (average power constraint is typically used in RF).
- In VLC, signal superposition may lead to the overlapping of multiple signals at the receiver, which in turn is a potential threat to integrity, authenticity and availability

The feasibility of conducting different types of attacks on VLC systems was discussed in [15]. In particular, with regard to availability and integrity requirements, the possibility of introducing a VLC jamming device was considered. This is difficult for mobile-to-mobile and fixed-to-mobile communication modes, but is achievable in the "infrastructure" scenario.

In this paper we will focus on VLC applications in office environments, where it is used as a primary or supplemental WLAN. In such an environment, the users are mobile and network coverage must be provided in the whole given area, hence multiple transmitters (APs) are used. A jamming attack in an infrastructure-type VLC system requires a rogue transmitter, and in general it is more difficult to introduce such a device into a VLC network than into a RF-based network, where it can be physically out of the users' eyesight. However, in installations with multiple transmitting luminaries, for example in multi-transmitter system based on femtocells, a malicious AP may easily pass undetected. Attackers may also try to "hijack" the VLC system via the network infrastructure backbone. In a large installation, such malicious intervention may pass undetected.

Theoretical rationale for VLC jamming was formulated in [16], where it was shown that a VLC signal source with sufficient transmission is able to to saturate the channel effectively obscuring the legitimate data source. The same effect may be achieved with the use of a number of hostile low-power transmitters.

C. Scope and structure of paper

In this paper we will focus on VLC systems used in office-type environments in an infrastructure mode, i.e. as a replacement or an augmentation for "traditional" RF-based WLANs. The possible scenarios for jamming attacks in office-based VLC systems were discussed in [17]. Here we develop further work presented in the above quoted paper and investigate mathematical models used to simulate the jamming process. A typical approach for computing the influence of the jammer assumes that all disruptive transmissions may be modeled as Gaussian noise. Contrastingly, in an "exact" model (first described by [18]), the full characteristics of the interfering signal are taken into account. The major contribution of this paper is a detailed comparison and benchmarking of both the Gaussian and the exact models, in order to determine which is adequate for studying signal jamming in VLC systems.

This paper is structured as follows: in section II we discuss the principles of VLC modeling and introduce Gaussian and exact models; in section III we describe the simulation technique and software; in section IV we present and discuss simulation results; and in section V we summarize the paper and outline areas of future research.

II. The Gaussian and exact models

A. Channel model

We will consider an indoor (office space) model with N fixed transmitters and a mobile receiver. The transmitter is an LED source, and the receiver a non-imaging photodetector. We will assume that On-Off-Keying (OOK) modulation is used, with "0" represented by completely turning off the light source and "1" by the source transmitting with some fixed power. We will also assume that the probabilities of the 0 and 1 symbols are equal to 50%. The master clock cycle is T, hence the bandwidth is: B ($B = \frac{1}{T}$). With this we can calculate bit error rate (BER), our major benchmarking factor, as:

$$BER = Q(\sqrt{SNR}) \tag{1}$$

where Q is the statistical Q-function defined as [19]:

$$Q(x) = \frac{1}{\sqrt{2\pi}} \int_x^\infty e^{\left(-\frac{u^2}{2}\right)} du$$

The signal received $Y(t)$ is given by:

$$Y(t) = R_p X(t) * h(t) + N(t) \tag{2}$$

where:

- $X(t)$ is the transmitted signal
- R_p is the receiver gain,
- $h(t)$ is the channel gain function,
- $N(t)$ is the channel and receiver noise,
- $*$ is the convolution operator.

We will calculate SNR as follows:

$$SNR = \frac{R_p^2 P_{recSignal}^2}{N} \tag{3}$$

where:

$$P_{recSignal} = \int_0^T (\sum_{i=1}^{N} h_i(t) * X(t) dt) \tag{4}$$

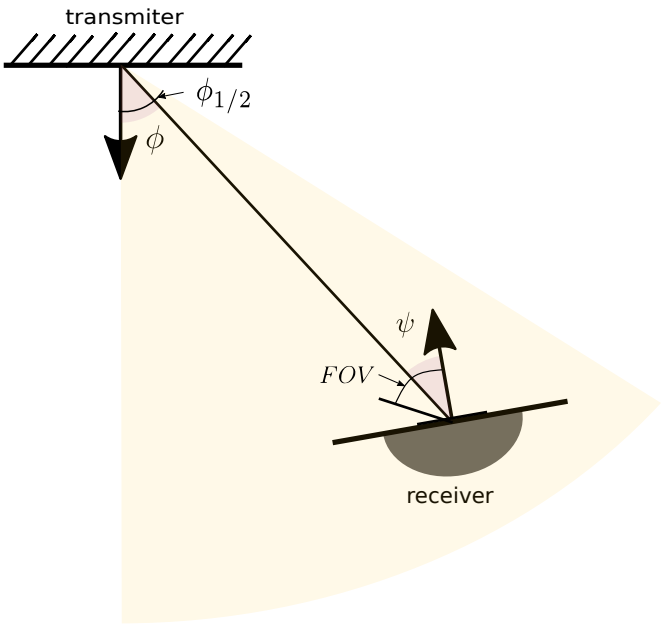

Fig. 1. Spacial arrangement of transmitter and receiver

N is the total noise power, given as:

$$N = \sigma^2_{shot} + \sigma^2_{thermal} + \sigma^2_{inter} \tag{5}$$

Shot noise is calculated as follows:

$$\sigma^2_{shot} = 2qR_pP_rB + 2qI_{bg}I_2 \tag{6}$$

where $P_r = P_{inter} + P_{recSignal}$. ($q$ is the elementary charge, and I_2 is the receiver characteristic constant.)

Interference noise is expressed by:

$$P_{inter} = \int_T^\infty (\sum_{i=1}^N h_i(t) * X(t)dt) \tag{7}$$

Thermal noise ($\sigma_{thermal}$) is determined mainly by the receiver's physical characteristics and some basic physical constants. To keep this discussion brief, we refer the reader to [3] for further details regarding the physical aspects of thermal noise calculation.

Now, we can introduce the formula for channel gain h which is derived from the geometrical model of the VLC channel, as first formulated in [3] The light sources are treated as Lambertian emitters. To calculate gain at the receiver's location we must account for the contribution of each light source. In the LoS model, only direct illumination is considered; in the NLoS model, light reflections from walls and other surfaces must be taken into account. In typical office conditions, the NLoS component contribution is typically below 5

$$h = H(0) = \frac{(m+1)A_r}{2\pi D^2}\cos^m(\phi)T(\psi)g(\psi)\cos\psi \tag{8}$$

where the m factor: $m = -\frac{\ln 2}{\ln(\cos\phi_{1/2})}$ is characteristic of the Lambertian emitter, and:

- A_r – area of the photodetector,
- ϕ is the angle of irradiance (see figure 1)
- ψ is the angle of incidence (see figure 1)
- $T(\psi)$ is the receiver filter gain,
- $g(\psi)$ is the receiver concentrator gain,
- D is the distance between a transmitter and receiver.

In a typical case of the receiver being placed on a flat surface facing upwards (towards the light source): $\psi = \phi$.

We will denote the bit sequence transmitted by transmitter j as $\{b_j^k\}_{k=-\infty}^{\infty}$, because OOK modulation b_j^k assumes only 0 and 1 values with equal probability. The signal at the transmitter can be expressed as:

$$X_j(t) = p_j \sum_{k=-\infty}^{k=\infty} b_j^k rect(t - kT) \tag{9}$$

where $rect(t)$ is the unit-amplitude rectangular pulse of duration T and p_i is the optical power of the emitter when transmitting symbol 1. The received signal is given as:

$$Y_i(t) = \sum_{j=1}^N R_p h_{ij} X_j(t - d_{ij}) + N_i(t) \tag{10}$$

where d_{ij} is the time delay between the transmitter j and receiver i[1], and N_i is the superposition of shot and thermal noise modeled as AWGN at the receivers' location. The channel gain h_{ij} is as expressed in eq. 8 assuming LoS between LED j and the receiver.

B. Demoduation model

For the purpose of exact modeling, we must focus on the detection process in the receiver in the presence of noise. At the receiver, the signal is demodulated with a matched filter. Demodulation is followed by a 0-or-1 decision with a threshold ξ. By $s_i^0(t)$ we denote the receiver–i impulse response with an amplitude of 1 and duration T. At this point we consider a scenario where transmitters and receivers are paired – $d_{ii} = 0$. We will introduce the case where multiple LEDs transmit simultaneously to one receiver later in this section. The first transmitted bit overlapping with the interval $[0, T)$ is b_j^0 and is followed by b_j^1, etc. Let $\tau_{ij} \in [0, 1)$ denote the time-normalized misalignment of b_j^0 and b_i^0. We assume that τ_{ij} is constant in the current transmitter–receiver configuration. After demodulation, the signal is expressed as:

$$\begin{aligned} y_i &= \frac{1}{T}\int_0^T r_i(t)s_i^0(t)dt \\ &= p_i h_{ii} R_p + \sum_{j\neq i} p_j h_{ij}(\tau_{ij}b_j^0 + (1-\tau_{ij})b_j^1)R_p + n_i \end{aligned} \tag{11}$$

where

$$n_i = \frac{1}{T}\int_0^T n_i(t)s_i^0(t)dt \tag{12}$$

[1]By receiver i, we understand the receiver located at some arbitrary location denoted as i.

represents AWGN with the distribution given by: $N(0, \sigma^2_{shot} + \sigma^2_{thermal})$.

To simplify, we will introduce $W_{ij} = \tau_{ij} b^0_j + (1 - \tau_{ij}) b^1_j$. Eq. 11 can be now rewritten as:

$$y_i = p_i h_{ii} R_p + \sum_{j \neq i} p_j h_{ij} W_{ij} R_p + n_i \tag{13}$$

Notice that W_{ij} is a discreet random variable taking values $\{\tau_{ij}, 1 - \tau_{ij}, 1, 0\}$ as illustrated in table I. In eq. 13 in the context of eqs. 4 and 7, the first sum component expresses the part of the signal transmitted by the "source" LED: $P_{recSignal} = p_i h_{ii} R_p$, while the second component is the interference generated by other LEDs – $P_{inter} = \sum_{j \neq i} p_j h_{ij} W_{ij} R_p$.

The noise component can be expressed as:

$$\begin{aligned} \sigma^2_{noise} &= \sigma^2_{shot} + \sigma^2_{thermal} \\ &= 2qR_p(p_i h_{ii} R_p + \sum_{j \neq i} p_j h_{ij} W_{ij})B \\ &+ 2qI_{bg} I_2 + \sigma^2_{thermal} \end{aligned} \tag{14}$$

TABLE I
POSSIBLE VALUES OF W_{ij} WITH RESPECT TO TRANSMITTED SYMBOLS.

W_{ij}	b^0_j	b^1_j
0	0	0
$1 - \tau_{ij}$	0	1
1	1	1
τ_{ij}	1	0

C. Exact model

In this subsection we present the exact analysis of BER as was first proposed by Chen et al. in [18]. In eq. 1, we substitute values of the received signal and noise power – eq. 3 according to the equations for power presented above. The transmission error occurs when "1" is classified by the receiver as "0" or "0" is classified as "1". This leads to two error "scenarios". The case where "0" is classified as "1", $p_i = 0$ ("0" is transmitted, hence 0 is substituted), for a given W_{ij} is expressed by eq. 20. The second case: "1" classified as "0", $p_i = p_t$, for a given W_{ij} is expressed by eq. 21. Eq. 15 lets us calculate exact BER for our model. The derivation of the exact model formula is presented in Appendix A

D. Decision threshold for the exact model

To determine the exact BER as expressed by eq. 15, we must compute the optimal decision threshold ξ. In general, this can only be done with the use of a one-dimensional search, but an approximate analytical formula was proposed [18] under the reasonable assumption that the data signal is larger than the aggregated interfering signals, so that ξ is in the range: $[\sum_{j \neq i} p_j h_{ij} R_p, p_i h_{ii} R_p]$. In the above cited work it was proven that the value of ξ minimizing BER is given by:

$$\begin{aligned} BER_{exact}(i) = \frac{1}{4^{N-1}} \sum_{W_{iN} \in \{\tau_{iN}, 1-\tau_{iN}, 0, 1\}} \cdots \sum_{W_{i1} \in \{\tau_{i1}, 1-\tau_{i1}, 0, 1\}} \\ \Big[\frac{1}{2} Q\Big(\frac{\xi_i - \sum_{j \neq i} p_j h_{ij} W_{ij} R_p}{\sqrt{2qR_p \sum_{j \neq i} p_j h_{ij} W_{ij} B + 2qI_{bg} I_2 + \sigma^2_{thermal}}}\Big) + \\ \frac{1}{2} Q\Big(\frac{(p_i h_{ii} + \sum_{j \neq i} p_j h_{ij} W_{ij}) R_p - \xi_i}{\sqrt{2qR_p (p_i h_{ii} + \sum_{j \neq i} p_j h_{ij} W_{ij}) B + 2qI_{bg} I_2 + \sigma^2_{thermal}}}\Big)\Big] \end{aligned} \tag{15}$$

$$\xi_i = \frac{1}{2}\Big(\sum_{j \neq i} p_j h_{ij} R_p + p_i h_{ii} R_p\Big) \tag{16}$$

E. Gaussian model

The formula for exact BER calculation – eq. 22 – with an exponentially growing number of sum components is not typically used. Instead it is common to treat all interference as white Gaussian noise. If in eq. 13 we approximate the term responsible for interference: $\sum_{j \neq i} p_j h_{ij} W_{ij} R_p$ with a Gaussian random variable, we obtain a much simpler *Gaussian interference model*. The expression for BER becomes:

$$\begin{aligned} BER_{gauss}(i) = \Big[\frac{1}{2} Q\Big(\frac{\xi_i - \frac{1}{2}\sum_{j \neq i} p_j h_{ij} R_p}{\sqrt{\sum_{j \neq i} p_j^2 h_{ij}^2 R_p^2 \Big(\frac{1}{2}\tau_{ij}^2 - \frac{1}{2}\tau_{ij} + \frac{1}{4}\Big) + 2qI_{bg} I_2 + \sigma^2_{thermal}}}\Big) + \\ \frac{1}{2} Q\Big(\frac{(p_i h_{ii} + \frac{1}{2}\sum_{j \neq i} p_j h_{ij}) R_p - \xi_i}{\sqrt{\sum_{j \neq i} p_j^2 h_{ij}^2 R_p^2 \Big(\frac{1}{2}\tau_{ij}^2 - \frac{1}{2}\tau_{ij} + \frac{1}{4}\Big) + 2qR_p p_i h_{ii} B + 2qI_{bg} I_2 + \sigma^2_{thermal}}}\Big)\Big] \end{aligned} \tag{17}$$

An outline of derivation of eq. **??** can be found in Appendix A. The formula obtained for simplified BER presented above is much simpler then eq. 15 because it eliminates the need to iterate over all interference components – all interfering sources are represented by one term instead.

F. Cooperating transmitters

The analysis presented in the preceding sections refers to the case where the receiver is paired with exactly one transmitter. However, for a practical scenario in which we would like to study the influence of one or more interfering transmitters, we must adjust the model to accommodate for a group of cooperating "legitimate" transmitters and one or more rogue transmitters. Such a configuration generates an additional condition expressed as:

$$ph = \sum_{k}^{parts} p_k h_k \tag{18}$$

This leads to the following:

- Legitimate transmitters are synchronized. Such an assumption is reasonable and has been demonstrated in practice for very high transmission bandwidth ranges [20].
- For synchronized transmitters we will ignore signal propagation delays, and in consequence inter-symbol interference (ISI). For a typical indoor scenario, this limits the transmission bandwidth to approx 100 Mb/s. (ISI is of course accounted for between groups of legitimate and rogue transmitters).
- When a rogue transmitter (or transmitters) is active, there are two possibilities: we are aware of this fact or we are not. This leads to a different approach in the analytical calculation of the threshold ξ. In the "a prior" (rogue aware) case, eqs. 15 and 17 should be applied and ξ calculated to account for the known interference. In the "a posteriori" case, ξ is computed as if no interference exists. The formula for the exact and Gaussian model is the same - eq. 19.

$$\begin{aligned} BER_{exact,nointer}(i) = BER_{gauss,nointer}(i) = \\ \frac{1}{2}Q\Big(\frac{\xi_i}{\sqrt{2qI_{bg}I_2 + \sigma^2_{thermal}}}\Big) + \\ \frac{1}{2}Q\Big(\frac{p_i h_{ii} R_p - \xi_i}{\sqrt{2qR_p p_i h_{ii} B + 2qI_{bg}I_2 + \sigma^2_{thermal}}}\Big) \end{aligned} \tag{19}$$

III. Simulation scenarios

In our simulations we considered a room of length 7.2 m, breadth 7.2 m and height 2.9 m. A receiver is placed at desk level, at a height of 1.25 m from the floor. The room dimensions are higher than those typically considered in similar models [21]–[23]. In our opinion, ours is a more realistic scenario reflecting true office spaces. The design of the scenario aims to provide ergonomic lighting conditions which meet current industry standards. The arrangement of luminaries and choice of their parameters is based on our previous work [17], where a discussion of modeling office VLC environments can also be found. The major difference between this and the above cited work is in the crucial issue of modeling interferences: in [17], both natural interference and hostile (i.e. jamming) luminaire influence is modeled simply with a normal Gaussian distribution, while in this work we are modeling the jamming influence with an exact model.

TABLE II
Simulation parameters – Receiver.

Parameter	Value
FOV	60°
Bandwidth	100 Mb/s
Area	10^{-4} m^2
Concentrator gain	$g(\psi) = \frac{1.5^2}{\sin FOV}$ for $\psi < FOV$ $g(\psi) = 0$ otherwise

The parameters of the room and the VLC system are given in tables II and III. Simulations were conducted for several different scenarios of luminaire arrangement with different choices of legitimate and rogue transmitters. The scenarios are as follows:

- **G1** – a 3x4 recessed luminaire grid – Fig. 2. This scenario represents the most common, standard solution for office spaces. One type of luminaire (type **g**) is used in this arrangement – a square 60 x 60 cm panel module with a 70 deg. radiation semi-angle.
- **G2** – a 2x4 recessed luminaire grid with an additional 1x3 array of downlight lower power elements – Fig. 2. This is an augmented version of G1, typical for office meeting rooms, open spaces, etc., with downlights providing additional illumination in recessed areas which are further from natural sources of light. Two types of luminaires are used in this and the next scenario: **g**-type used in scenario G1 and lower-power luminaires – **d** with a more narrow radiation semi-angle of 30 deg.
- **GC** – a 2 x 3 luminaire grid surrounded by a circular arrangement of lower power downlight elements – Fig. 3. Such an arrangement is used in rooms with little or no access to natural light. This scenario also provides a more uniform light distribution in the room perimeter, which is a favorable feature for VLC communication.

In figures 2 – 4, the scale is in meters, and the numbered dots represent individual luminaries. For each scenario: G1, G2 and GC, a set of rogue transmission arrangements was simulated:

- **G1** – rogue transmitters are: independently g7 or g10, or simultaneously both g7 and g10.

TABLE III
SIMULATION PARAMETERS – LUMINAIRES.

Luminaire type	g	d
LED irradiance semi-angle at half power	70°	30°
Luminous flux	2000 lm	1600 lm

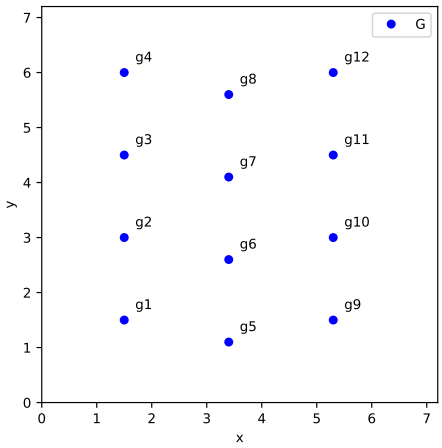

Fig. 2. Scenario **G1** – a 3x4 recessed luminaire grid.

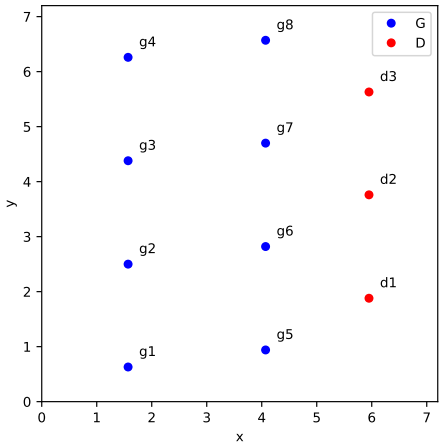

Fig. 3. Scenario **G2** – a 2x4 recessed luminaire grid with an additional 1x3 array of downlight lower power elements.

- **G2** – rogue transmitters are: d2 or d1, d2, d3 (simultaneously).
- **GC** – rogue transmitters are: d1 – d5 (simultaneously) or d6 – d10 (simultaneously).

All tests were conducted in both in the a priori and a posteriori scenarios (see section II-F).

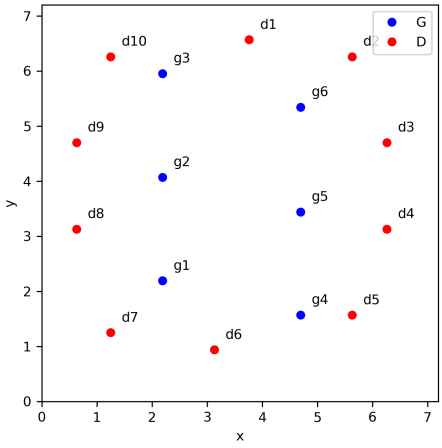

Fig. 4. Scenario **GC** – a 2 x 3 luminaire grid with an additional circular arrangement of lower power downlight elements.

IV. SIMULATION RESULTS

A. Scenario G1

The simulation results for scenario G1 are shown in figures 5 – 7. Isolines indicate BER levels of: 10^{-2}, 10^{-3}, 10^{-5}. These values were chosen based on the fact that the BER level of 10^{-3} is the maximum limit for voice-type transmission and the level of 10^{-5} is the maximum for data transmission with FEC (Forward Error Correction). Black isolines are relevant to the Gaussian model and red ones to the exact model (the same also applies to subsequent simulation scenarios G2 and GC).

Let us analyze the first case with one rogue transmitter located in the center – fig. 5. In the "a priori case" (i.e. when we anticipate that the given transmitter is rogue) it is possible to compensate for the presence of the rogue transmitter by adjusting the threshold value ξ, hence there are no red isolines for this case (left diagram). For the "a posteriori" case (right diagram) we can observe the influence of the rogue transmitter. Furthermore, for the exact model, the increased BER value due to g7 interference is more contained than for the Gaussian model. From this case we can conclude that the exact model shows slightly lower levels of interference (with respect to the affected room area) than the Gaussian model. In the exact model, approx. 10% of the total area exhibits BER in the range of 10^{-3} or larger. This is 28% in the Gaussian model.

In the second simulation, the rogue transmitter is located next to the wall – fig. 6. The area affected is larger than in the previous case and in the "a priori" variant, higher BER levels can be observed. This is due to the fact that there is a smaller number of legitimate transmitters in the vicinity which can compensate for the rogue one. In the exact model, approx. 16% of the total area exhibits BER in the range of 10^{-3} or larger; in the Gaussian model this is 30%. Again we can conclude that for the exact model, the increased BER value due to interference is more contained than for the

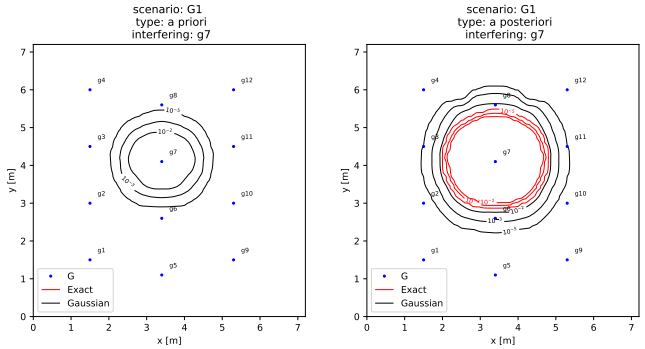

Fig. 5. Simulation for the G1 scenario, rogue transmitter is g7. Left: "a priori" case, right: "a posteriori" case.

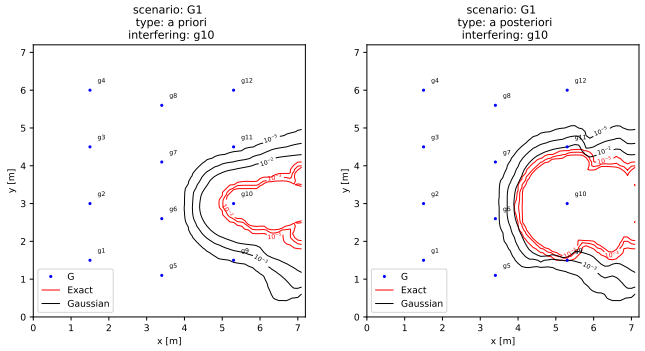

Fig. 6. Simulation for the G1 scenario, rogue transmitter is g10. Left: "a priori" case, right: "a posteriori" case.

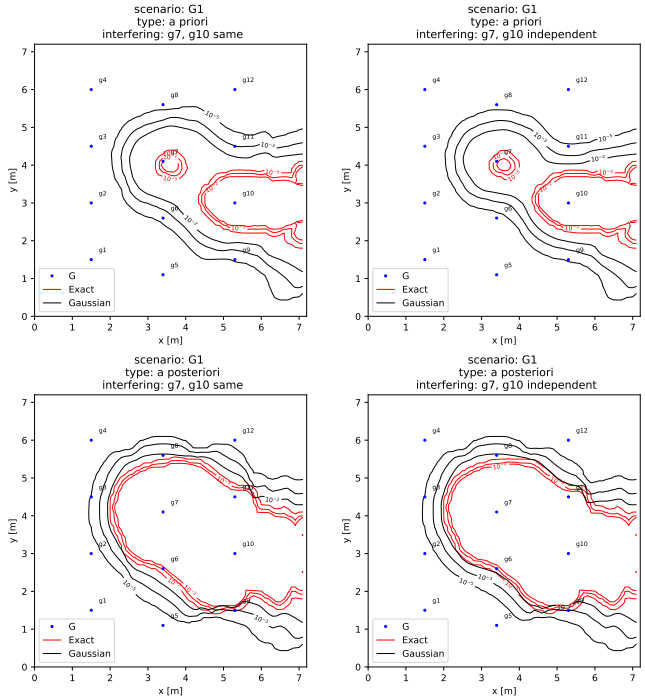

Fig. 7. Simulation for the G1 scenario, rogue transmitters are g7 and g10. Left: g7 and g10 are synchronized; right: g7 and g10 are independent. Top two diagrams represent "a priori" case, bottom "a posteriori".

Gaussian model.

The next simulation considers a case when two transmitters are rogue. We have chosen g7 and g10, with two alternatives of independence between them or full synchronization. The results are shown in fig. 7. Here we can make the following observations:

- As in the previous test case, the exact model shows slightly lower levels of interference (with respect to the affected room area) than the Gaussian model.
- Rather obviously, the overall influence of two rogue transmitters is larger than one; in the exact model and the "a priori" variant, it is not possible to compensate for the joint influence of g7 and g10 in the vicinity of g7 (refer to fig. 5).
- In the case of synchronized rogue transmitters (graphs on the left), in the Gaussian model the area influenced by rogue transmitters is larger than in the case of independent transmitters (graphs on the right) both in the "a priori" and "a posteriori" case. This is in accordance with intuition – the effect of synchronized rogue transmitters should be stronger than the effect of independent ones.
- A similar but weaker effect can be observed in the exact model.
- The more realistic "a posteriori" (no knowledge of the rogue transmission) shows a significantly larger influence of the rogue transmitters. Again, the area affected is smaller in the exact model, but still approx. 27% of the whole area shows BER in the range of 10^{-3} or larger, and in the Gaussian model, the influenced area is 43%.

B. Scenario G2

The placement of luminaries in this scenario is similar to the previous one, but less homogeneous – instead of a regular 3 x 4 grid of identical transmitters, a 2 x 4 grid is used augmented with a "line" of narrow-angled emitters by the wall. The introduction of a different set of emitters makes the possibility of their physical takeover more likely. We can also assume that such downlight emitters could be installed for the sole purpose of introducing rogue transmitters. We will analyze two cases: with one rogue emitters – fig. 8 – and with three rogue emitters (all d-type emitters are rogue) – fig. 9. The influence of d-type emitters is more local because of their narrow angle.

- As in the previous test cases, the exact model shows slightly lower levels of interference (with respect to the affected room area) than the Gaussian model.
- There is no visible difference between "a priori" and "a posteriori" cases. This is due to the lower power and lower semiangle values of the rogue luminaries.
- Perhaps surprisingly, there is no difference in results obtained for synchronized and independent transmitters. This is because of the narrow angle of luminaire "d". However, this limitation becomes critical in different luminaire arrangement models.
- In the exact model for one rogue transmitter and the "a posteriori" case, the area affected by rogue transmission

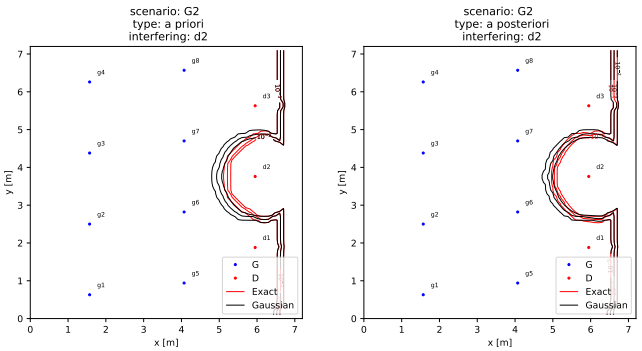

Fig. 8. Simulation for the G2 scenario, rogue transmitter is d2. Left: "a priori" case, right "a posteriori".

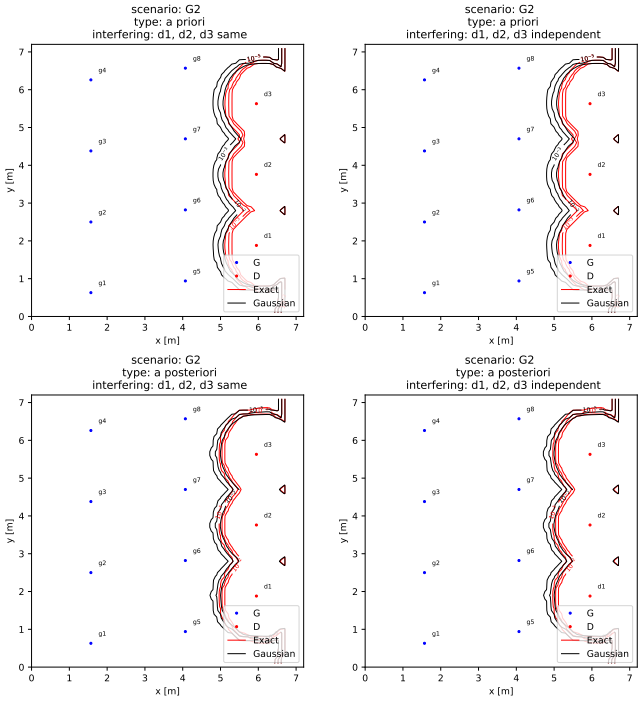

Fig. 9. Simulation for the G2 scenario, rogue transmitters are d1, d2, d3. Left: rogue transmitters are synchronized; right: rogue transmitters are independent. Top two diagrams represent "a priori" case, bottom "a posteriori" case.

occupies approx. 6% of the whole area. For three transmitters, the area affected is 20%.

C. Scenario GC

In this scenario, we assume that some of the d-type luminaires have become rogue. Note that the d-type luminaire has different characteristics than the g-type: it has lower power, and more importantly a narrower illuminance half-angle, hence its influence is more "local". The simulation results are shown in fig. 10. The following observations can be made:

- As in the previous test cases, the exact model shows slightly lower levels of interference (with respect to the affected room area) than the Gaussian model,
- There is a smaller difference between "a priori" and "a posteriori" cases in this simulation than in G1. This is caused by lower power and lower semiangle values of the rogue luminaries.
- As in G2, there is no difference in results obtained for synchronized and independent transmitters.
- In the exact model and "a posteriori" case, the area affected by rogue transmission occupies approx. 14% of the whole area; in the Gaussian model this is 17%.

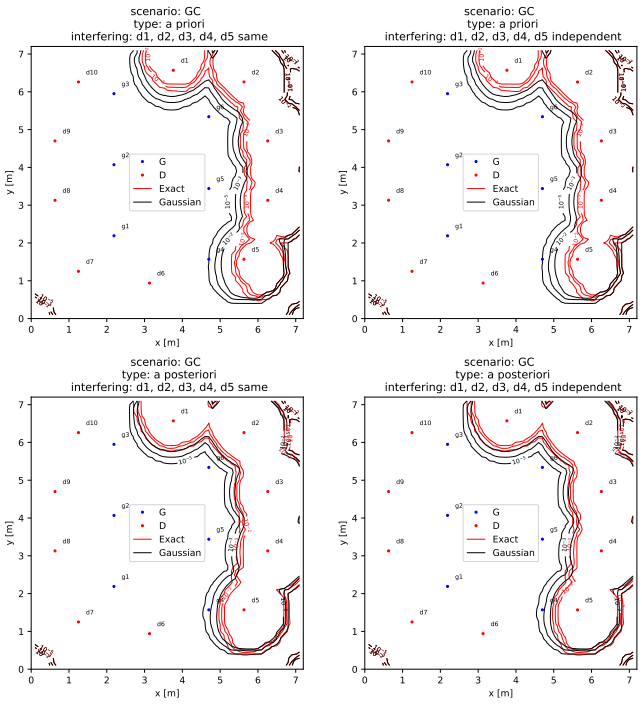

Fig. 10. Simulation for the GC scenario, rogue transmitters are d1 – d5. Left: rogue transmitters are synchronized; right: rogue transmitters are independent. Top two diagrams represent "a priori" case, bottom "a posteriori" case.

It is worth mentioning here that in scenarios with a larger number of luminaries, "a priori" calculation become very time-consuming. This is because of the time needed to find the ξ threshold in the exact model: increasing the number of rogue transmitters by one increases the time needed 4-fold.

V. Conclusions

In this work, we have presented a numerical study of a VLC system with rogue transmitters. We have compared two numerical models used to simulate VLC environments: a **Gaussian model** in which rogue transmitters are treated as yet another source of white noise interference, and an **exact model** in which the full characteristics of the interfering signal are taken into account. Both models were tested by comparing simulation results in three different scenarios (luminaire arrangements), each with two kinds of rogue transmitter placement. Additionally we have tested two ways of approaching the rogue transmission – in an "a priori" case, where the system is aware of the rogue transmitter and tries to compensate for its influence by altering the detection threshold, and in a more realistic "a posteriori" case, where there is no knowledge about rogue transmission placement and number. The conclusions are as follows:

Both models show similar patterns of raised BER levels; the exact model is more "optimistic" – the areas affected by interfering transmitters are 10% – 50% smaller according to the particular scenario. The exact model's simulation can become very time-consuming with an increasing number of rogue transmitters because of the complexity of the algorithm used to find the ξ threshold, but this is only the case in the a priori approach. In general, the exact model is more numerically complex and we can conclude that in practical cases using the simpler Gaussian model would suffice, as it gives a "worst case estimate" of the area affected by rogue transmitter(s).

APPENDIX A
DERIVATION OF FORMULAS FOR EXACT AND GAUSSIAN MODELS

The formula for BER in the exact model is calculated as follows (refer to section II-C):

$$\begin{aligned}
P_{err}(y_i > \xi | b_i^0 = 0) &= Q\Big(\frac{\xi_i - R_p P_r}{\sqrt{\sigma^2_{noise}}}\Big) \\
&= Q\Big(\frac{\xi_i - (p_i h_{ii} + \sum_{j\neq i} p_j h_{ij} W_{ij}) R_p}{\sqrt{\sigma^2_{shot} + \sigma^2_{thermal}}}\Big) \\
&= Q\Big(\frac{\xi_i - (p_i h_{ii} + \sum_{j\neq i} p_j h_{ij} W_{ij}) R_p}{\sqrt{\sigma^2_{shot} + \sigma^2_{thermal}}}\Big) \\
&= Q\Big(\frac{\xi_i - (p_i h_{ii} + \sum_{j\neq i} p_j h_{ij} W_{ij}) R_p}{\sqrt{2qR_p(p_i h_{ii} R_p + \sum_{j\neq i} p_j h_{ij} W_{ij})B + 2qI_{bg}I_2 + \sigma^2_{thermal}}}\Big) \\
&\overset{2}{=} Q\Big(\frac{\xi_i - \sum_{j\neq i} p_j h_{ij} W_{ij} R_p}{\sqrt{2qR_p \sum_{j\neq i} p_j h_{ij} W_{ij} B + 2qI_{bg}I_2 + \sigma^2_{thermal}}}\Big)
\end{aligned} \tag{20}$$

$$P_{err}(y_i \leq \xi | b_i^0 = 0) = Q\Big(\frac{(p_i h_{ii} + \sum_{j\neq i} p_j h_{ij} W_{ij}) R_p - \xi_i}{\sqrt{2qR_p(p_i h_{ii} + \sum_{j\neq i} p_j h_{ij} W_{ij})B + 2qI_{bg}I_2 + \sigma^2_{thermal}}}\Big). \tag{21}$$

Eqs. 20 and 21 represent BER for a given value of W_{ij}. To obtain the final formula, we must take the average over all possible combinations of W_{ij}, i.e.: 4^{N-1} cases. This is expressed by eq. 22

$$\begin{aligned}
BER_{exact}(i) = \frac{1}{4^{N-1}} &\sum_{W_{iN}\in\{\tau_{iN}, 1-\tau_{iN}, 0, 1\}} \cdots \sum_{W_{i1}\in\{\tau_{i1}, 1-\tau_{i1}, 0, 1\}} \\
&\Big[\frac{1}{2} Q\Big(\frac{\xi_i - \sum_{j\neq i} p_j h_{ij} W_{ij} R_p}{\sqrt{2qR_p \sum_{j\neq i} p_j h_{ij} W_{ij} B + 2qI_{bg}I_2 + \sigma^2_{thermal}}}\Big) + \\
&\frac{1}{2} Q\Big(\frac{(p_i h_{ii} + \sum_{j\neq i} p_j h_{ij} W_{ij}) R_p - \xi_i}{\sqrt{2qR_p(p_i h_{ii} + \sum_{j\neq i} p_j h_{ij} W_{ij})B + 2qI_{bg}I_2 + \sigma^2_{thermal}}}\Big)\Big]
\end{aligned} \tag{22}$$

The formula for BER in the Gaussian model is calculated as follows (refer to section II-E):

We treat the interference component – $\sum_{j\neq i} p_j h_{ij} W_{ij} R_p$ – as a Gaussian random variable, with mean m and variance σ_I^2 calculated as follows:

All possible values of W_{ij} are contained in: $\{\tau_{ij}, 1 - \tau_{ij}, 1, 0\}$, where each element occurs with the same probability, hence:

$$m = \sum_{j\neq i} p_j h_{ij} R_p \frac{\tau_{ij} + 1 - \tau_{ij} + 1 + 0}{4}) = \frac{1}{2} \sum_{j\neq i} p_j h_{ij} R_p \tag{23}$$

The variance is derived as follows:

$$\begin{aligned}
\sigma_I^2 &= \sum_{j\neq i} p_j^2 h_{ij}^2 R_p^2 \Big(\frac{(\tau_{ij} - \frac{1}{2})^2 + (1 - \tau_{ij} - \frac{1}{2})^2 + (1 - \frac{1}{2})^2 + (0 - \frac{1}{2})^2}{4}\Big) \\
&= \sum_{j\neq i} p_j^2 h_{ij}^2 R_p^2 \Big(\frac{1}{2}\tau_{ij}^2 - \frac{1}{2}\tau_{ij} + \frac{1}{4}\Big)
\end{aligned} \tag{24}$$

REFERENCES

[1] G. Pang, K.-L. Ho, T. Kwan, and E. Yang, "Visible light communication for audio systems," *IEEE Transactions on Consumer Electronics*, vol. 45, no. 4, pp. 1112–1118, 1999.

[2] Y. Tanaka, S. Haruyama, and M. Nakagawa, "Wireless optical transmissions with white colored led for wireless home links," in *Personal, Indoor and Mobile Radio Communications, 2000. PIMRC 2000. The 11th IEEE International Symposium on*, vol. 2. IEEE, 2000, pp. 1325–1329.

[3] T. Komine and M. Nakagawa, "Fundamental analysis for visible-light communication system using LED lights," *IEEE Transactions on Consumer Electronics*, vol. 50, no. 1, pp. 100–107, 2004.

[4] D. C. O'Brien, L. Zeng, H. Le-Minh, G. Faulkner, J. W. Walewski, and S. Randel, "Visible light communications: Challenges and possibilities," in *2008 IEEE 19th International Symposium on Personal, Indoor and Mobile Radio Communications*, Sept 2008, pp. 1–5.

[5] H. Le Minh, D. O'Brien, G. Faulkner, L. Zeng, K. Lee, D. Jung, and Y. Oh, "High-speed visible light communications using multiple-resonant equalization," *IEEE Photonics Technology Letters*, vol. 20, no. 14, pp. 1243–1245, 2008.

[6] H. Elgala, R. Mesleh, and H. Haas, "Indoor optical wireless communication: potential and state-of-the-art," *IEEE Communications Magazine*, vol. 49, no. 9, 2011.

[7] A. H. Azhar, T. Tran, and D. O'Brien, "A gigabit/s indoor wireless transmission using mimo-ofdm visible-light communications," *IEEE photonics technology letters*, vol. 25, no. 2, pp. 171–174, 2013.

[8] M. S. Islim, R. X. Ferreira, X. He, E. Xie, S. Videv, S. Viola, S. Watson, N. Bamiedakis, R. V. Penty, I. H. White *et al.*, "Towards 10 gb/s orthogonal frequency division multiplexing-based visible light communication using a gan violet micro-led," *Photonics Research*, vol. 5, no. 2, pp. A35–A43, 2017.

[9] P. H. Pathak, X. Feng, P. Hu, and P. Mohapatra, "Visible light communication, networking, and sensing: A survey, potential and challenges," *IEEE Communications Surveys Tutorials*, vol. 17, no. 4, pp. 2047–2077, Fourthquarter 2015.

[10] L. U. Khan, "Visible light communication: Applications, architecture, standardization and research challenges," *Digital Communications and Networks*, vol. 3, no. 2, pp. 78–88, 2017.

[11] e. a. Samsung Electronics, "Visible Light Communication," *Tutorial*, 2008. [Online]. Available: http://www.ieee802.org/802_tutorials/2008-03/15-08-0114-02-0000-VLC_Tutorial_MCO_Samsung-VLCC-Oxford_2008-03-17.pdf

[12] K.-D. Langer, J. Grubor, O. Bouchet, M. El Tabach, J. W. Walewski, S. Randel, M. Franke, S. Nerreter, D. C. O'Brien, G. E. Faulkner *et al.*, "Optical wireless communications for broadband access in home area networks," in *Transparent Optical Networks, 2008. ICTon 2008. 10th Anniversary International Conference on*, vol. 4. IEEE, 2008, pp. 149–154.

[13] M. Yoshino, S. Haruyama, and M. Nakagawa, "High-accuracy positioning system using visible led lights and image sensor," in *Radio and Wireless Symposium, 2008 IEEE*. IEEE, 2008, pp. 439–442.

[14] C. B. Liu, B. Sadeghi, and E. W. Knightly, "Enabling vehicular visible light communication (v2lc) networks," in *Proceedings of the Eighth ACM international workshop on Vehicular inter-networking*. ACM, 2011, pp. 41–50.

[15] G. Blinowski, "Security issues in visible light communication systems," *IFAC-PapersOnLine*, vol. 48, no. 4, pp. 234–239, 2015.

[16] G. J. Blinowski, "Practical Aspects of Physical and MAC Layer Security in Visible Light Communication Systems," *International Journal of Electronics and Telecommunications*, vol. 62, no. 1, pp. 7–13, 2016.

[17] ——, "The feasibility of launching rogue transmitter attacks in indoor visible light communication networks," *Wireless Personal Communications*, vol. 97, no. 4, pp. 5325–5343, 2017.

[18] Y. Chen, C. W. Sung, S. W. Ho, and W. S. Wong, "BER analysis for interfering visible light communication systems," in *2016 10th International Symposium on Communication Systems, Networks and Digital Signal Processing, CSNDSP 2016*, 2016.

[19] M. Abramowitz, I. A. Stegun, and R. H. Romer, "Handbook of Mathematical Functions with Formulas, Graphs, and Mathematical Tables," *American Journal of Physics*, vol. 56, no. 10, pp. 958–958, 1988. [Online]. Available: http://aapt.scitation.org/doi/10.1119/1.15378

[20] O. Abari, H. Rahul, and D. Katabi, "Poster: Clock synchronization for distributed wireless protocols at the physical layer," in *Proceedings of the 20th annual international conference on Mobile computing and networking*. ACM, 2014, pp. 337–340.

[21] M. Nakagawa, "Visible light communications," in *Proc. Conference on Lasers and Electro-Optics/Quantum Electronics and Laser Science Conference and Photonic Applications Systems Technologies, Baltimore*, 2007.

[22] K. Cui, J. Quan, and Z. Xu, "Performance of indoor optical femtocell by visible light communication," *Optics Communications*, vol. 298, pp. 59–66, 2013.

[23] A. Mostafa and L. Lampe, "Physical-layer security for indoor visible light communications," in *Communications (ICC), 2014 IEEE International Conference on*. IEEE, 2014, pp. 3342–3347.